The Vortex Lattice in Conventional and High-T_c Superconductors

Ernst Helmut Brandt

Max-Planck-Institut für Metallforschung, D-70506 Stuttgart, Germany

Some properties of the flux-line lattice in conventional and high-T_c superconductors are reviewed, with particular stress on phenomenological theories, nonlocal elasticity, irreversible magnetization curves, and influence of the specimen shape on the electromagnetic response.

I. Introduction

After the discovery of superconductivity in 1912 by Heike Kamerlingh-Onnes in Leiden, it took almost 50 years until this fascinating phenomenon was understood microscopically, when in 1957 Bardeen, Cooper and Schrieffer established the BCS theory. But long before this, there were powerful phenomenological theories, which were able to explain most electromagnetic and thermodynamic observations on superconductors, and which are very useful also today [1, 2, 3]. The London theory of 1935 is particularly useful for the description of the high-T_c superconductors, which were discovered in 1987 by Bednorz and Müller. The Ginzburg-Landau (GL) theory of 1951 is quite universal; it contains the London theory as particular limit and predicts that superconductors can be of type-I (with positive energy of the wall between normal conducting and superconducting domains) or of type-II (with negative wall energy, pointing to an instability).

The penetration of vortices into type-II superconductors was predicted first by A. A. Abrikosov when he discovered a two-dimensional periodic solution of the Ginzburg-Landau (GL) equations. Abrikosov correctly interpreted this solution as a periodic arrangement of flux lines, the flux-line lattice (FLL). Each flux line (or fluxon, vortex line) carries one quantum of magnetic flux $\Phi_0 = h/2e = 2.07 \cdot 10^{-15}$ Tm^2, which is caused by the supercurrents circulating in this vortex. The magnetic field peaks at the vortex positions. The vortex core is a tube in which the superconductivity is weakened; the position of the vortex is defined by the line at which the superconducting order parameter vanishes. For well separated or isolated vortices, the radius of the tube of magnetic flux equals the magnetic penetration depth λ, and the core ra-

dius is somewhat larger than the superconducting coherence length ξ [1, 2, 3], see Fig. 1. With increasing applied magnetic field, the spacing a_0 of the vortices decreases and the average flux density $\bar{B}$ increases, one has $\bar{B} = 2\Phi_0/(\sqrt{3}a_0^2)$ for the triangular FLL, see Fig. 2. The flux tubes then overlap such that the periodic induction $B(x, y)$ is nearly constant, with only a small relative variation about its average $\bar{B}$. With further increase of $\bar{B}$ also the vortex cores begin to overlap such that the amplitude of the order parameter decreases until it vanishes when $\bar{B}$ reaches the upper critical field $B_{c2} = \mu_0 H_{c2} = \Phi_0/(2\pi\xi^2)$, where the superconductivity disappears. Fig. 3 shows profiles of the induction $B(x, y)$ and of the order parameter $|\psi(x, y)|^2$ for two values of $\bar{B}$ corresponding to flux-line spacings $a_0 = 4\lambda$ and $a_0 = 2\lambda$.
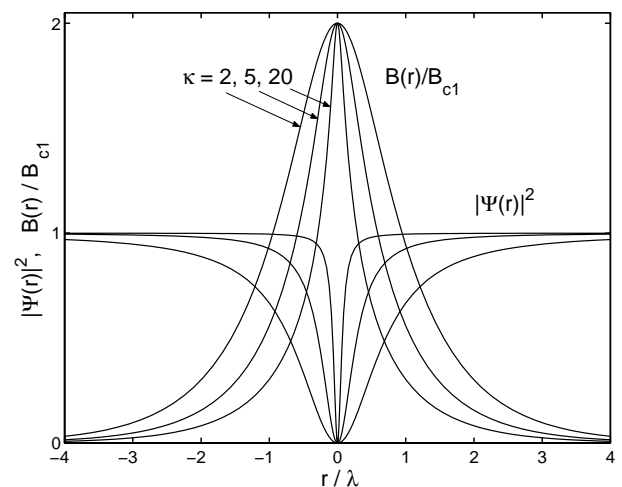

Figure 1. Magnetic field $B(r)$ and order parameter $|\psi(r)|^2$ of an isolated flux line calculated from Ginzburg-Landau theory for Ginzburg-Landau parameters $\kappa = 2$, 5, and 20.
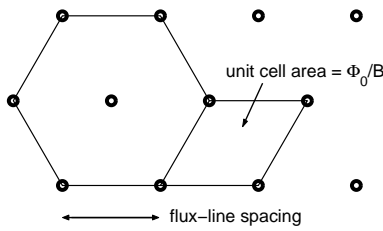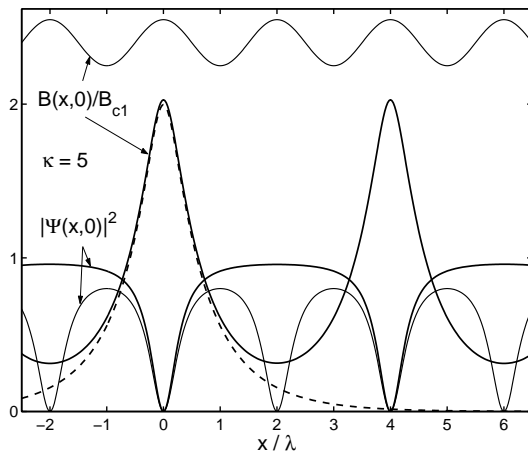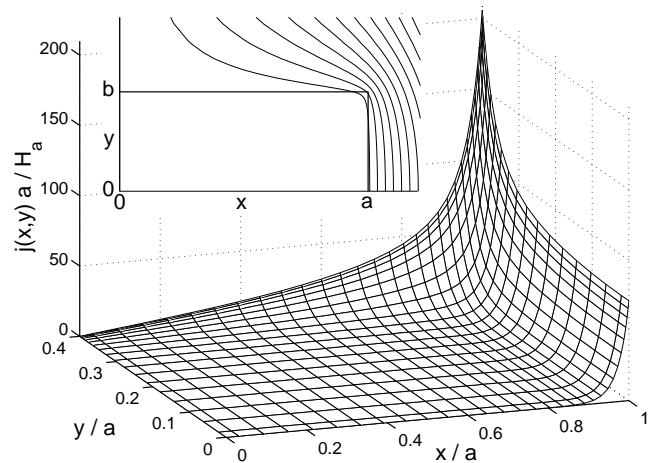
Figure 2. The triangular flux-line lattice.

Figure 4. A strip with aspect ratio $b/a = 0.4$ in the Meissner state with London penetration depth $\lambda = 0.025a_0$ in a perpendicular magnetic field H_a. Shown is the current density in a quarter of the cross section and the magnetic field lines (inset).

Figure 3. Two profiles of the magnetic field $B(x,y)$ and order parameter $|\Psi(x,y)|^2$ along the x axis (a nearest neighbor direction) for flux-line lattices with lattice spacings $a = 4\lambda$ (solid lines) and $a = 2\lambda$ (thin lines). The dashed line shows the magnetic field of an isolated flux line from Fig. 1. Calculations from Ginzburg-Landau theory for $\kappa = 5$.

In long slabs or cylinders, with increasing parallel field $H_a > H_{c1}$, vortices penetrate and the inner induction $\bar{B}$ increases monotonically. The magnetization in this longitudinal geometry is defined as $M = \bar{B}/\mu_0 - H_a$, Fig. 5. The negative magnetization $-M$ initially increases linearly, $M = -H_a$ ($H_a = B_a/\mu_0$) for $H_a \leq H_{c1}$ (Meissner state); at $H_a = H_{c1}$, $-M$ decreases sharply since flux lines start to penetrate; and when H_a is increased further, $-M$ decreases approximately linearly until it vanishes at H_{c2}. The area under the magnetization curve $-M(H_a)$ is $\mu_0 H_c^2$, where $B_c = \mu_0 H_c = \Phi_0/(\sqrt{8}\pi\xi\lambda) = B_{c2}/(\sqrt{2}\kappa)$ is the thermodynamic critical field. In superconductors with $\kappa = 1/\sqrt{2}$ (this case is almost exactly realized in pure Niobium) the three critical fields coincide, $H_{c1} = H_c = H_{c2}$.

The periodic solution which describes the FLL exists when the GL parameter $\kappa = \lambda/\xi$ exceeds the value $1/\sqrt{2}$ (this condition defines type-II superconductors) and when the applied magnetic field $B_a = \mu_0 H_a$ ranges between the lower critical field $B_{c1} = \mu_0 H_{c1} \approx \Phi_0 \ln(\sqrt{2}\kappa)/(4\pi\lambda^2)$ (where $\bar{B} = 0$) and B_{c2} (where $\bar{B} = B_a = B_{c2}$). For $|B_a| < B_{c1}$ the superconductor is in the Meissner state, which expels all magnetic flux, forcing $B \equiv 0$ inside the superconductor. More precisely, for $B_a < B_{c1}$ [and in type-I superconductors with $\kappa < 1/\sqrt{2}$ for $B_a < B_c = \Phi_0/(\sqrt{8}\pi\xi\lambda)$], the applied magnetic field penetrates into a surface layer of thickness λ. For a superconducting half space at $x > 0$ one has $B(x) = B_a \exp(-x/\lambda)$. For a long strip with rectangular cross section ($|x| \leq a = 40\lambda$, $|y| \leq b = 0.4a$) and with B_a along y, Fig. 4 shows that in this surface layer both $B(x,y)$ and the screening current density $J(x,y) = \mu_0^{-1}\nabla \times \mathbf{B}(x,y)$ (flowing along z) are sharply peaked in the corners, favoring the nucleation and penetration of vortices in form of quarter loops at the four corners of the strip [4, 5].
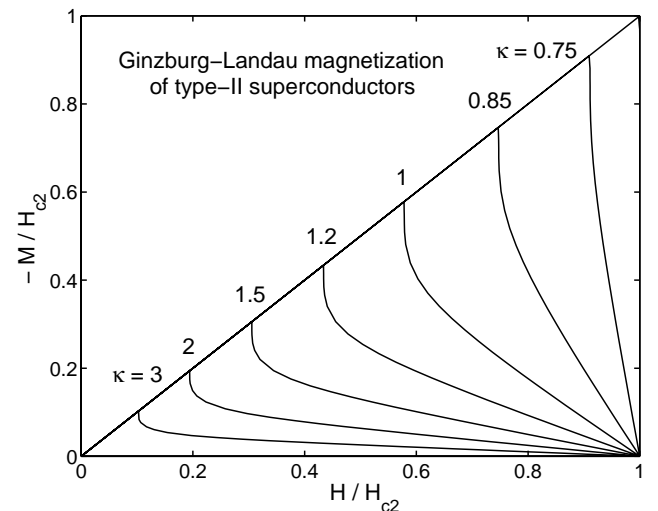

Figure 5. Magnetization curves $M(H)$ of long type-II superconductors in parallel magnetic field H (demagnetization factor $N = 0$) calculated from Ginzburg-Landau theory for various Ginzburg-Landau parameters $\kappa = 0.75 \ldots 3$. For $\kappa = 1/\sqrt{2}$, $-M$ jumps vertically from $-M = H$ to $M = 0$ at $H = H_{c1} = H_{c2}$.

The GL theory originally was derived for temperatures T close to the superconducting transition temperature T_c, where $\lambda \propto \xi \propto (1 - T/T_c)^{-1/2}$ diverges. But practically the GL picture is a good approximation at all temperatures $0 < T < T_c$, in particular in impure superconductors with short electron mean free path. One usually assumes the temperature dependences $\lambda(T) \approx \lambda(0)(1 - t^4)^{-1/2}$ (with $t = T/T_c$) and $H_c(T) \approx H_c(0)(1 - t^2)$, yielding $\xi(T) \approx \xi(0)[(1 + t^2)/(1 - t^2)]^{1/2}$.

At low inductions $\bar{B} \ll B_{c2}$ and large $\kappa \gg 1$, the properties of the vortex lattice may be calculated from London theory, to which the GL theory reduces when the magnitude $|\psi|$ of the GL function ψ is nearly constant. In the London limit, $B(x, y)$ is the linear superposition of the fields of isolated vortices; the London expressions for $B(x, y)$ and for the energy apply thus also to nonperiodic arrangements of vortices. The London theory was further extended to curved vortices and to anisotropic superconductors. At larger $\bar{B} > 0.25 B_{c2}$ or smaller $\kappa < 2$, the GL theory has to be used. Analytic GL solutions are available only for the periodic FLL near B_{c2}, but not for a distorted FLL or at lower $\bar{B}$.

Expanding the energy of the superconductor with respect to small displacements of the vortices from their ideal lattice positions, one obtains the elastic moduli of the vortex lattice. As opposed to the local elasticity of atomic lattices, the elasticity of the vortex lattice is *nonlocal* [3], i.e., the energy of compressional and tilt deformations is strongly reduced when the wave vector k of the strain field is large, $k > \lambda^{-1}$, see Sct. 4.

II. Results from London Theory

The London theory may be formulated by minimizing the sum F of the potential energy of the magnetic field $\mathbf{B}(\mathbf{r})$ and the kinetic energy of the supercurrent density $\mathbf{J}(\mathbf{r}) = \mu_0^{-1} \nabla \times \mathbf{B}(\mathbf{r})$,

$$F = \frac{1}{2\mu_0} \int_V [\mathbf{B}^2 + \lambda^2 (\nabla \times \mathbf{B})^2] \, \mathrm{d}^3 r \,, \qquad (1)$$

with respect to $\mathbf{B} = \nabla \times \mathbf{A}$. This yields the homogeneous London equation $\mathbf{B} - \lambda^2 \nabla^2 \mathbf{B} = 0$ or $\mathbf{J} = -\mu_0^{-1} \lambda^{-2} \mathbf{A}$ where the Maxwell equations $\nabla \cdot \mathbf{B} = 0$ and $\nabla \times \mathbf{B} = \mu_0 \mathbf{J}$ were used and the vector potential $\mathbf{A}$ was chosen in the "London gauge" $\nabla \cdot \mathbf{A} = 0$.

A. Parallel vortices

In the presence of vortices one has to add singularities which describe the vortex core. For straight parallel vortex lines along $\hat{\mathbf{z}}$ one thus gets the modified London equation

$$\mathbf{B}(\mathbf{r}) - \lambda^2 \nabla^2 \mathbf{B}(\mathbf{r}) = \hat{\mathbf{z}} \, \Phi_0 \sum_\nu \delta_2(\mathbf{r} - \mathbf{r}_\nu) \,. \qquad (2)$$

Here $\mathbf{r}_\nu = (x_\nu, y_\nu)$ are the two-dimensional (2D) vortex positions and $\delta_2(\mathbf{r}) = \delta(x)\delta(y)$ is the 2D delta function. This linear equation may be solved by Fourier transform using $\int \exp(i\mathbf{kr}) d^2k = 4\pi^2 \delta_2(\mathbf{r})$ and $\int \exp(i\mathbf{kr})(k^2 + \lambda^{-2})^{-1} d^2k = 2\pi K_0(|\mathbf{r}|/\lambda)$. Here $K_0(x)$ is a modified Bessel function with the limits $K_0(x) \approx -\ln(x)$ for $x \ll 1$ and $K_0(x) \approx (\pi/2x)^{1/2} \exp(-x)$ for $x \gg 1$. The resulting magnetic field of any arrangement of parallel vortices is the sum of individual vortex fields centered at the positions $\mathbf{r}_\nu$,

$$\mathbf{B}(\mathbf{r}) = \hat{\mathbf{z}} \frac{\Phi_0}{2\pi\lambda^2} \sum_\nu K_0 \left(\frac{|\mathbf{r} - \mathbf{r}_\nu|}{\lambda} \right) , \qquad (3)$$

see Fig. 1. The energy F_{2D} of this 2D arrangement of vortex lines with length L is obtained by inserting Eq. (2) into (1). Integrating over the delta function one finds that the London energy is determined by the magnetic field values at the vortex positions,

$$\begin{aligned} F_{2D} &= L \frac{\Phi_0}{2\mu_0} \sum_\mu B(\mathbf{r}_\mu) \\ &= L \frac{\Phi_0^2}{4\pi\mu_0\lambda^2} \sum_\mu \sum_\nu K_0 \left(\frac{|\mathbf{r}_\mu - \mathbf{r}_\nu|}{\lambda} \right) . \quad (4) \end{aligned}$$

This expression shows that the energy is composed of the self-energy of the vortices (terms $\mu = \nu$) and a pairwise interaction energy (terms $\mu \neq \nu$). To avoid the divergence of the self-energy one has to cut off the logarithmic infinity of B at the vortex centers $\mathbf{r}_\nu$ by introducing a finite radius of the vortex core of order ξ, the coherence length of the GL theory. This cutoff may be achieved by replacing in Eq. (4) the distance $r_{\mu\nu} = |\mathbf{r}_\mu - \mathbf{r}_\nu|$ by $\tilde{r}_{\mu\nu} = (r_{\mu\nu}^2 + 2\xi^2)^{1/2}$ and multiplying by a normalization factor ≈ 1 to conserve the flux Φ_0 of the vortex. This analytical expression suggested by Clem [6] for a single vortex and later generalized to the vortex lattice [7], is an excellent approximation, as was shown numerically [8] by solving the GL equation for the periodic FLL in the entire range of $\bar{B}$ and κ, for $0 \le \bar{B} \le B_{c2}$ and $\kappa \ge 1/\sqrt{2}$.

B. Curved vortices

Arbitrary 3D arrangements of curved vortices at positions $\mathbf{r}_\nu(z) = [x_\nu(z), y_\nu(z), z]$ satisfy the 3D London equation [3]

$$\mathbf{B}(\mathbf{r}) - \lambda^2 \nabla^2 \mathbf{B}(\mathbf{r}) = \Phi_0 \sum_\nu \int d\mathbf{r}_\nu \, \delta_3(\mathbf{r} - \mathbf{r}_\nu) \,. \qquad (5)$$

Here the integral is along the vortex lines and $\delta_3(\mathbf{r}) = \delta(x)\delta(y)\delta(z)$. The resulting magnetic field and energy are, with $\tilde{r}_{\mu\nu} = [|\mathbf{r}_\mu(z) - \mathbf{r}_\nu(z)|^2 + 2\xi^2]^{1/2}$,

$$\mathbf{B}(\mathbf{r}) = \frac{\Phi_0}{4\pi\lambda^2} \sum_\nu \int d\mathbf{r}_\nu \frac{\exp[-\tilde{r}_{\mu\nu}(\mathbf{r}_\mu = \mathbf{r})/\lambda]}{\tilde{r}_{\mu\nu}(\mathbf{r}_\mu = \mathbf{r})} , \quad (6)$$

$$F_{3D} = \frac{\Phi_0}{2\mu_0} \sum_\mu \int d\mathbf{r}_\mu B(\mathbf{r}_\mu)$$

$$= \frac{\Phi_0^2}{8\pi\mu_0\lambda^2} \sum_\mu \sum_\nu \int d\mathbf{r}_\mu \int d\mathbf{r}_\nu \frac{\exp(-\tilde{r}_{\mu\nu}/\lambda)}{\tilde{r}_{\mu\nu}}.$$

This means all the vortex segments interact with each other similar as magnetic dipoles or tiny current loops, but the magnetic long-range interaction $\propto 1/r$ is screened by a factor $\exp(-\tilde{r}_{\mu\nu}/\lambda)$. The 3D interaction between curved vortices is visualized in Fig. 6.
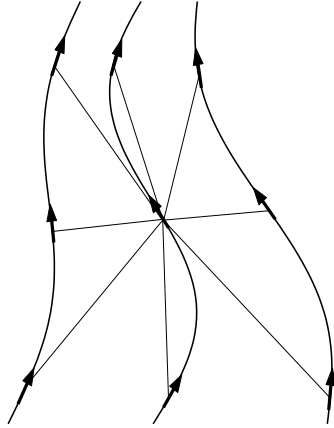
Interaction between curved flux lines

Figure 6. Visualization of the pairwise interaction between all line elements (arrows) of curved flux lines within London theory, Eqs. (6) and (7).

C. Vortices near a surface

The solutions (6) apply to vortices in the bulk. Near the surface of the superconductor these expressions have to be modified. In simple geometries, e.g. for superconductors with one or two planar surfaces surrounded by vacuum, the magnetic field and energy of a given vortex arrangement is obtained by adding the field of appropriate images (in order to satisfy the boundary condition that no current crosses the surface) and a magnetic stray field which is caused by a fictitious surface layer of magnetic monopoles and which makes the total magnetic field continuous across the surface [9]. The magnetic field and interaction of straight vortices oriented perpendicular to a superconducting film of arbitrary thickness is calculated in Ref. [10, 11].

D. Thin Films and Layered Superconductors

Near the surface of a superconductor the self and interaction energies are modified. In films of thickness $d \ll \lambda$ the short 2D vortices interact mainly via their magnetic stray field outside the superconductor over an effective penetration depth $\Lambda = 2\lambda^2/d$. At short distances $r \ll \Lambda$ this interaction is logarithmic as in the bulk case, and at large $r \gg \Lambda$ it decreases as $\exp(-r/\Lambda)$. With decreasing thickness d, the Fourier transform of the 2D vortex interaction

$V(r) = \int (d^2k/4\pi^2)\tilde{V}(k)\exp(i\mathbf{kr})$ changes from $\tilde{V}(k) = E_0(k^2 + \lambda^{-2})^{-1}$ ($d \gg \lambda$) to $\tilde{V}(k) = E_0(k^2 + k\Lambda^{-1})^{-1}$ ($d \ll \lambda$) where $E_0 = d\Phi_0^2/(\mu_0\lambda^2)$. A similar (but 3D) magnetic interaction exists between the 2D pancake vortices [12] in the superconducting CuO layers of high-T_c superconductors, $\tilde{V}(\mathbf{k}) = E_0\,d\,k_3^2\,k_2^{-2}\,(\lambda^{-2} + k_3^2)^{-1}$, where now d is the distance between the layers, $k_2^2 = k_x^2 + k_y^2$, $k_3^2 = k_2^2 + k_z^2$, and $\lambda = \lambda_{ab}$ is the penetration depth for currents flowing in these layers [12, 3].

E. Anisotropic Superconductors

For many purposes high-T_c superconductors may be considered as uniaxially anisotropic materials, which within London theory are characterized by two penetration depths $\lambda_a \approx \lambda_b \approx \lambda_{ab}$ (for currents in the ab plane) and λ_c (for currents along the c axis). The anisotropy ratio $\Gamma = \lambda_c/\lambda_{ab} = \xi_{ab}/\xi_c \geq 1$ describes also the anisotropy of the GL coherence lengths, ξ_{ab} and ξ_c, which are needed as inner cutoff lengths in the anisotropic London theory. The general solution for arbitrarily arranged straight or curved vortex lines is [3]

$$B_\alpha(\mathbf{r}) = \Phi_0 \sum_\mu \int d\mathbf{r}_\mu^\beta \, f_{\alpha\beta}(\mathbf{r} - \mathbf{r}_\mu) \tag{7}$$

$$F_{3D} = \frac{\Phi_0^2}{2\mu_0} \sum_\mu \sum_\nu \int d\mathbf{r}_\mu^\alpha \int d\mathbf{r}_\nu^\beta f_{\alpha\beta}(\mathbf{r}_\mu - \mathbf{r}_\nu)$$

with the tensorial interaction ($\alpha, \beta = x, y, z$)

$$f_{\alpha\beta}(\mathbf{r}) = \int \frac{d^3k}{8\pi^3} \, \exp(i\mathbf{kr}) \, f_{\alpha\beta}(\mathbf{k}) \tag{8}$$

$$f_{\alpha\beta}(\mathbf{k}) = \frac{\exp[-2g(k,q)]}{1 + \Lambda_1 k^2} \left(\delta_{\alpha\beta} - \frac{q_\alpha \, q_\beta \, \Lambda_2}{1 + \Lambda_1 k^2 + \Lambda_2 q^2}\right).$$

Here $g(k,q) = \xi_{ab}^2 q^2 + \xi_c^2(k^2 - q^2) = (\Lambda_1 k^2 + \Lambda_2 q^2)\xi_c^2/\lambda_{ab}^2$ enters the cutoff factor $\exp(-2g)$; $\mathbf{q} = \mathbf{k} \times \hat{\mathbf{c}}$, $\hat{\mathbf{c}}$ is the unit vector along the c-axis, $\Lambda_1 = \lambda_{ab}^2$, $\Lambda_2 = \lambda_c^2 - \lambda_{ab}^2 \geq 0$, and the sums and integrals are over the μth and νth vortex line. Due to the tensorial character of $f_{\alpha\beta}(\mathbf{r})$ the contribution of the segment $d\mathbf{r}_\mu$ to $\mathbf{B}(\mathbf{r})$ now in general is not parallel to $d\mathbf{r}_\mu$.

III. Ginzburg-Landau, Pippard, and BCS Theories

The London theory was extended in two ways, which both introduce a second length ξ: The Ginzburg-Landau (GL) theory is nonlinear in ψ and the Pippard theory is nonlocal in $\mathbf{A}$. All three theories later were shown to follow from the microscopic BCS theory in limiting cases.

A. Ginzburg-Landau Theory

The GL theory of 1950 introduces a complex order parameter $\psi(\mathbf{r})$ in addition to the magnetic field

$\mathbf{B}(\mathbf{r}) = \nabla \times \mathbf{A}(\mathbf{r})$. The GL function $\psi(\mathbf{r})$ is proportional to the BCS energy-gap function $\Delta(\mathbf{r})$, and its square $|\psi(\mathbf{r})|^2$ to the density of Cooper pairs. The superconducting coherence length ξ gives the scale over which $\psi(\mathbf{r})$ can vary, while λ governs the variation of the magnetic field as in London theory. Both λ and ξ diverge at the superconducting transition temperature T_c according to $\lambda \propto \xi \propto (T_c - T)^{-1/2}$, but their ratio, the GL parameter $\kappa = \lambda/\xi$, is nearly independent of the temperature T. The GL theory reduces to the London theory (which is valid down to $T = 0$) in the limit $\xi \ll \lambda$, which means constant magnitude $|\psi(\mathbf{r})| =$ const, except in the vortex cores, where ψ vanishes. The GL equations are obtained by minimizing a free energy functional $F\{\psi, \mathbf{A}\}$ with respect to the GL function $\psi(\mathbf{r})$ and the vector potential $\mathbf{A}(\mathbf{r})$. With the length unit λ and magnetic field unit $\sqrt{2}B_c$ the GL functional reads

$$F\{\psi, \mathbf{A}\} = \frac{B_c^2}{\mu_0} \int \Big[-|\psi|^2 + \frac{1}{2}|\psi|^4$$
$$+ |(-\frac{i\nabla}{\kappa} - \mathbf{A})\psi|^2 + (\nabla \times \mathbf{A})^2 \Big] \, \mathrm{d}^3 r \,. \qquad (9)$$

This functional and the resulting GL equations may be expressed in terms of the real function $|\psi|$ and the gauge-invariant supervelocity $\nabla\varphi/\kappa - \mathbf{A}$ where $\varphi(\mathbf{r})$ is the phase of $\psi = |\psi|\exp(i\varphi)$. The supercurrent density is $\mathbf{J} = \mu_0^{-1}\lambda^2(\nabla\varphi/\kappa - \mathbf{A})|\psi|^2$. In an external field $\mathbf{H_a}$ one has to minimize not the free energy F but the Gibbs free energy $G = F - \bar{\mathbf{B}}\mathbf{H_a}$. The condition $\partial G/\partial\bar{\mathbf{B}}$ yields the equilibrium field $\mathbf{H_a} = \partial F/\partial\bar{\mathbf{B}}$. The reversible magnetization curves $\bar{B}(H_a)$ of pin-free superconductors, Fig. 5, were calculated in this way from GL theory [8], together with the profiles of Fig. 3.

The GL theory modifies the London interaction between vortices in two ways: (a) The range of the magnetic repulsion at large inductions $\bar{B}$ becomes larger, $\lambda' = \lambda/(1 - \bar{B}/B_{c2})^{1/2}$. (b) A weak attraction of range $\xi' = \xi/(2 - 2\bar{B}/B_{c2})^{1/2}$ is added, caused by the condensation energy that is gained by the overlap of the vortex cores. Parallel vortex lines then interact by an effective potential $V(r) \propto K_0(r/\lambda') - K_0(r/\xi')$ which no longer diverges at zero distance r [13].

B. Pippard Theory

Inspired by Chamber's nonlocal generalization of Ohm's law, Pippard 1953 introduced a superconductor coherence length ξ by generalizing the London equation $\mu_0\mathbf{J} = -\lambda_L^{-2}\mathbf{A}$ to a nonlocal relationship [2]

$$\mu_0\mathbf{J}(\mathbf{r}) = -\lambda_P^{-2} \frac{3}{4\pi\xi^2} \int \frac{\mathbf{r}'(\mathbf{r}'\mathbf{A}(\mathbf{r} - \mathbf{r}'))}{r'^3} \, e^{-r'/\xi} \mathrm{d}^3 r'. \quad (10)$$

In the presence of electron scattering with mean free path l, the Pippard penetration depth $\lambda_P = (\lambda_L^2 \xi_0/\xi)^{1/2}$ exceeds the London penetration depth λ_L of a pure material with coherence length ξ_0, since

the effective coherence length ξ is reduced by scattering, $\xi^{-1} \approx \xi_0^{-1} + l^{-1}$ [2]. In the limit of small $\xi \ll \lambda_P$, Eq. (10) reduces to the local relation $\mu_0\mathbf{J}(\mathbf{r}) = -\lambda_P^{-2}\mathbf{A}(\mathbf{r})$. In Fourier space Pippard's Eq. (10) reads $\mu_0\mathbf{J}(\mathbf{k}) = -Q_P(k)\mathbf{A}(\mathbf{k})$ with

$$Q_P(k) = \lambda_P^{-2} h(k\xi),$$
$$h(x) = \frac{3}{2x^3}\Big[(1 + x^2)\mathrm{atan}\,x - x\Big], \quad h(0) = 1\,. \quad (11)$$

This Pippard theory is useful mainly for superconductors with small GL parameter κ.

BCS Theory

The microscopic BCS theory (in the Green function formulation of Gor'kov) for weak magnetic fields yields a similar nonlocal relation $\mu_0\mathbf{J}(\mathbf{k}) = -Q(k)\mathbf{A}(\mathbf{k})$ as suggested by Pippard, replacing the Pippard kernel $Q_P(k)$ by the BCS kernel [14, 3]

$$Q_{\mathrm{BCS}}(k) = \lambda^{-2}(T) \sum_{n=1}^{\infty} \frac{h[k\xi_K/(2n+1)]}{1.0518\,(2n+1)^3}\,. \quad (12)$$

Here $h(x)$ is defined in Eq. (11), $\lambda(T) = Q_{\mathrm{BCS}}(0)^{-1/2} \approx \lambda(0)(1 - T^4/T_c^4)^{-1/2}$ is the temperature dependent magnetic penetration depth, and $\xi_K = \hbar v_F/(2\pi k_B T) \approx 0.844\lambda(T)T_c/(\kappa T)$ (v_F = Fermi velocity, κ = GL parameter). The range of the BCS Gorkov kernel is of the order of the BCS coherence length $\xi_0 = \hbar v_F/(\pi\Delta_0)$ where Δ_0 is the BCS energy gap at $T = 0$.

With the nonlocal relation $\mu_0\mathbf{J}(\mathbf{k}) = -Q(k)\mathbf{A}(\mathbf{k})$ the Eq. (2) for a vortex line at $\mathbf{r}_\nu = 0$ now becomes $[1 + Q(k)^{-1}k^2]\tilde{B}(k) = \Phi_0$ with the solution

$$\tilde{B}(k) = \frac{\Phi_0\,Q(k)}{Q(k) + k^2},$$
$$B(r) = \frac{\Phi_0}{2\pi} \int_0^{\infty} \frac{Q(k)}{Q(k) + k^2} J_0(kr)\,k\,\mathrm{d}k\,, \quad (13)$$

where $J_0(x)$ is a Bessel function. The Pippard or BCS field $B(r)$ (13) of an isolated vortex line is no longer monotonic as compared with the London field, cf. Eq. (3), but it exhibits a field reversal with a negative minimum at large distances $r \gg \lambda_P$ from the vortex core. This effect should be observable if $\xi \approx \lambda$, i.e., for clean superconductors with small GL parameter κ at low temperatures. See also recent work on this nonlocal electrodynamics [15].

The field reversal of the vortex field is partly responsible for the attractive interaction between flux lines at large distances, which was observed in clean Niobium at temperatures not too close to T_c and which follows from BCS theory at $T < T_c$ for pure superconductors with GL parameter κ close to $1/\sqrt{2}$. This attraction leads to abrupt jumps in the magnetization curve and to an agglomeration of flux lines that can be observed in superconductors with demagnetization factor $N \neq 0$

as FLL islands surrounded by Meissner state, or Meissner islands surrounded by FLL [16]. For the definition of N see Sec. 5.

Another BCS effect which differs from the GL result is that in clean superconductors at low temperatures the periodic magnetic field $B(x, y)$ of the FLL near B_{c2} is not a smooth spatial function as in GL theory, but has sharp conical maxima and minima such that the profile $B(x, 0)$ along a nearest neighbor direction has zig-zag shape [3]. The reason for this is that the electron mean free path in pure superconductors at $T \to 0$ becomes larger than the vortex spacing a_0. This leads to a slow decrease of the Fourier coefficients $B_{\mathbf{K}} \propto (-1)^{m+mn+n} K_{mn}^{-3}$ of $B(x, y)$, while at $T \approx T_c$ the GL theory near B_{c2} yields a rapid decrease, $B_{\mathbf{K}} \propto (-1)^{m+mn+n} \exp(-K_{mn}^2 x_1 y_2/8\pi)$. Here $\mathbf{K} = \mathbf{K}_{mn} = (2\pi/x_1 y_2)(my_2; -mx_2 + nx_1)$ ($m, n = 1, 2, 3, \ldots$) are the reciprocal lattice vectors of the ideal vortex lattice with positions $\mathbf{R}_{mn} = (mx_1 + nx_2; ny_2)$, and $x_1 y_2 = \Phi_0/\bar{B}$ is the area of the unit cell, see Fig. 2.

IV. Elasticity of the Vortex Lattice

The flux-line displacements caused by pinning forces and by thermal fluctuations may be calculated using the elasticity theory of the FLL. Fig. 7 visualizes the three basic distortions of the triangular FLL: shear, uniaxial compression, and tilt. The linear elastic energy F_{elast} of the FLL is obtained by expanding its free energy F with respect to small displacements $\mathbf{u}_\nu(z) = \mathbf{r}_\nu(z) - \mathbf{R}_\nu = (u_{\nu x}, u_{\nu y})$ of the flux lines from their ideal parallel lattice positions $\mathbf{R}_\nu$ and keeping only the quadratic terms. This yields [3]

$$F_{\mathrm{elast}} = \frac{1}{2} \int_{\mathrm{BZ}} \frac{\mathrm{d}^3 k}{8\pi^3} u_\alpha(\mathbf{k}) \, \Phi_{\alpha\beta}(\mathbf{k}) \, u_\beta^*(\mathbf{k}) \qquad (14)$$

where $\mathbf{u}(\mathbf{k})$ is the Fourier transform of the displacement field $\mathbf{u}_\nu(z)$, now $(\alpha, \beta) = (x, y)$, and $\mathbf{k} = (k_x, k_y, k_z)$. The k-integral in Eq. (14) is over the first Brillouin zone (BZ) of the FLL since the "elastic matrix" $\Phi_{\alpha\beta}(\mathbf{k})$ is periodic in the k_x, k_y plane; the finite vortex core radius restricts the k_z integration to $|k_z| \le \xi^{-1}$. For an elastic medium with uniaxial symmetry the elastic matrix reads

$$\Phi_{\alpha\beta}(\mathbf{k}) = (c_{11} - c_{66})k_\alpha k_\beta$$
$$+ \delta_{\alpha\beta}[(k_x^2 + k_y^2)c_{66} + k_z^2 c_{44}]. \qquad (15)$$

The coefficients c_{11}, c_{66}, and c_{44} are the elastic moduli of uniaxial compression, shear, and tilt, respectively. For the FLL, $\Phi_{\alpha\beta}(\mathbf{k})$ was calculated from GL and London theories [3]. The result, a sum over reciprocal lattice vectors, should coincide with expression (15) in the continuum limit, i.e., for small $|\mathbf{k}| \ll k_{BZ}$, where $k_{BZ} = (4\pi\bar{B}/\Phi_0)^{1/2}$ is the radius of the circularized (actually hexagonal) Brillouin zone of the triangular

FLL with area πk_{BZ}^2. In the *London limit* one finds for isotropic superconductors the elastic moduli

$$c_{11}(k) \approx \frac{\bar{B}^2/\mu_0}{1 + k^2\lambda^2}, \quad c_{66} \approx \frac{\bar{B}\Phi_0/\mu_0}{16\pi\lambda^2},$$
$$c_{44}(\mathbf{k}) \approx c_{11}(k) + 2c_{66} \ln \frac{\kappa^2}{1 + k_z^2\lambda^2}. \qquad (16)$$

The *GL theory* yields an additional factor $(1 - \bar{B}/B_{c2})^2$ in c_{66}, i.e., $c_{66} \propto \bar{B}(\bar{B} - B_{c2})^2$, and replaces λ in $c_{11}(k)$ by λ' [17, 8]. The $\mathbf{k}$ dependence (dispersion) of the compression and tilt moduli $c_{11}(k)$ and $c_{44}(\mathbf{k})$ means that the elasticity of the vortex lattice is *nonlocal*, i.e., strains with short wavelengths $2\pi/k \ll 2\pi\lambda$ have a much lower elastic energy than a homogeneous compression or tilt (corresponding to $\mathbf{k} \to 0$). This elastic nonlocality comes from the fact that the magnetic interaction between the flux lines typically has a range λ much longer than the flux-line spacing a_0, therefore, each flux line interacts with many other flux lines. Note that large λ causes a small shear stiffness since $c_{66} \propto \lambda^{-2}$, Eq. (16), and a smaller $c_{11}(k > \lambda^{-1})$, but the uniform compressibility $c_{11}(k = 0)$ is independent of λ.
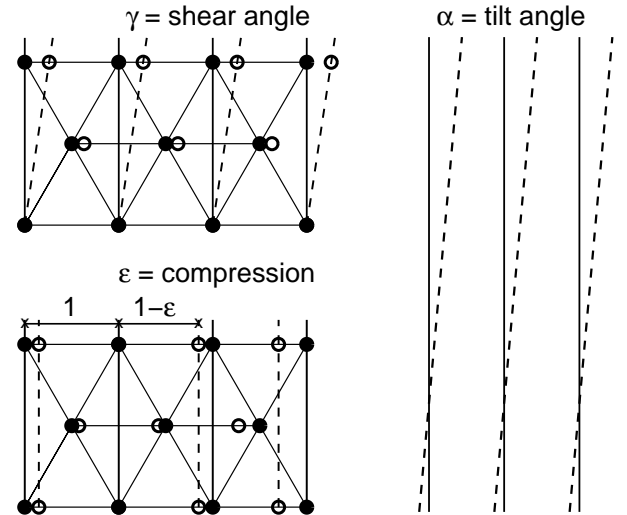

Figure 7. The three basic homogeneous elastic distortions of the triangular flux-line lattice. The full dots and solid lines mark the ideal lattice and the hollow dots and dashed lines the distorted lattice.

The compressional modulus c_{11} and the typically much smaller shear modulus $c_{66} \ll c_{11} \approx c_{44}$ originate from the flux-line interaction, but the last term in the tilt modulus c_{44} (16) originates from the line tension of isolated flux lines, defined by $P = \lim_{\bar{B} \to 0}(c_{44}\Phi_0/\bar{B})$. In isotropic (or cubic) superconductors like Nb and its alloys, the line tension P coincides with the self energy F_s of a flux line, $P = F_s$, $F_s = \Phi_0 H_{c1} \approx (\Phi_0^2/4\pi\mu_0\lambda^2)(\ln \kappa + 0.5)$ for $\kappa \gg 1$. In anisotropic materials the line tension and line energy of flux lines in general are different and depend on the angle θ of the vortex line with respect to the c-axis. One has

$P(\theta) = F_s(\theta) + \partial^2 F_s/\partial\theta^2$. Using $F_s(\theta) = F_s(0)(\cos^2\theta + \Gamma^{-2}\sin^2\theta)^{1/2}$ with $\Gamma = \lambda_c/\lambda_{ab} \geq 1$, one obtains $P(0) = F_s(0)/\Gamma^2$ and $P(\pi/2) = F_s(\pi/2)\Gamma^2 = P(0)/\Gamma^3$ (for tilt out of the ab-plane) [3]. In isotropic superconductors the uniaxial symmetry of the ideal vortex lattice, i.e., the appearance of a preferred axis, is induced by the applied magnetic field. This induced anisotropy leads to a small difference between the compressional and tilt moduli c_{11} and c_{44}, but not to a difference between line energy and line tension.

As a consequence of nonlocal elasticity, the flux-line displacements $\mathbf{u}_\nu(z)$ caused by local pinning forces, and also the space and time averaged thermal fluctuations $\langle \mathbf{u}_\nu(z)^2 \rangle$, are much larger than they would be if $c_{44}(\mathbf{k})$ had no dispersion, i.e., if it were replaced by $c_{44}(0) = \bar{B}H_a \approx \bar{B}^2/\mu_0$. The maximum vortex displacement $u(0) \propto f$ caused at $\mathbf{r} = 0$ by a point force of density $f\delta_3(\mathbf{r})$, and the thermal fluctuations $\langle u^2 \rangle \propto k_B T$, are given by similar expressions [3],

$$\frac{2u(0)}{f} \approx \frac{\langle u^2 \rangle}{k_B T} \approx \int_{BZ} \frac{d^3 k}{8\pi^3} \frac{1}{(k_x^2 + k_y^2)c_{66} + k_z^2 c_{44}(\mathbf{k})}$$
$$\approx \frac{k_{BZ}^2 \lambda}{8\pi[c_{66}c_{44}(0)]^{1/2}} . \quad (17)$$

In this result a large factor $[c_{44}(0)/c_{44}(k_{BZ})]^{1/2} \approx k_{BZ}\lambda \approx \pi\lambda/a \gg 1$ originates from the elastic non-locality. In anisotropic superconductors with $B \| c$, the thermal fluctuations (17) are enhanced by an additional factor $\Gamma = \lambda_c/\lambda_{ab}$ [3]. For an exact analytic evaluation of the integral (17) for $\langle u^2 \rangle$ see [18].

V. High-T_c Superconductors

The nonlocal elastic response of the vortex lattice is particularly important for understanding the thermodynamic and electrodynamic properties of the high-T_c superconductors, which were discovered in 1987 and the following years. These oxides with high superconducting transition temperature T_c (e.g. $YBa_2Cu_3O_{7-\delta}$ with $T_c = 92.5$ K, $Bi_2Sr_2Ca_2Cu_3O_{10+\delta}$ with $T_c = 120$ K, and some Hg and Tl compounds with even higher T_c) are layered structures with more or less decoupled superconducting Cu-O layers. They thus exhibit high anisotropy of their superconducting properties. For example, YBCO has an anisotropy $\Gamma = 5$ and BSCCO has $\Gamma \approx 100$. This means in BSCCO the layers are almost decoupled and the penetration depth λ_c for currents flowing along the c axis is macroscopically large, $\lambda_c = \Gamma\lambda_{ac}$ with $\lambda_{ab} \approx 140$ nm at $T = 0$. Therefore, the magnetic field component parallel to the layers penetrates easily.

This large λ_c also causes very pronounced elastic nonlocality, which means a very soft vortex lattice. The vortices are thus strongly pinned collectively, since the vortex lattice adjusts to the pins, but at higher temperatures they are easily depinned by thermal activation,

since the elementary pinning energy of very flexible vortices is small. By the same token, thermal fluctuations of the vortices are large and may even cause melting of the vortex lattice into a vortex liquid.

The effects of the elastic nonlocality and anisotropy on the thermal fluctuation, melting, and pinning of the FLL are treated in detail in the review [19], where also phase diagrams in the H_a-T plane are presented for 3D and layered superconductors. Phase diagrams obtained by applying simple Lindemann criteria ($\langle u^2 \rangle = c_L^2 a_0^2$, $c_L \approx 0.25$) to both thermal and pinning-caused fluctuations in 3D superconductors at not too low fields ($\bar{B} > B_{c1}$) are calculated in [20], namely, the line $H_m(T)$ where the FLL melts, the line $H_{sv}(T)$ which separates the regimes of single-vortex-pinning and of vortex-bundle-pinning, and the order–disorder line $H_{dis}(T)$ above which pinning causes plastic deformation of the FLL, see Fig. 8. In this case ($B = \mu_0 H$, no decoupling of layers) the phase diagram in reduced units $H_a/H_{c2}(0)$ and $t = T/T_c$, depends only on the Ginzburg number Gi and on the pinning strength $D = [J_c(0)/J_0(0)]^{1/2}$ (critical current for $B \to 0$ over the depairing current, both at $T = 0$), see [20].
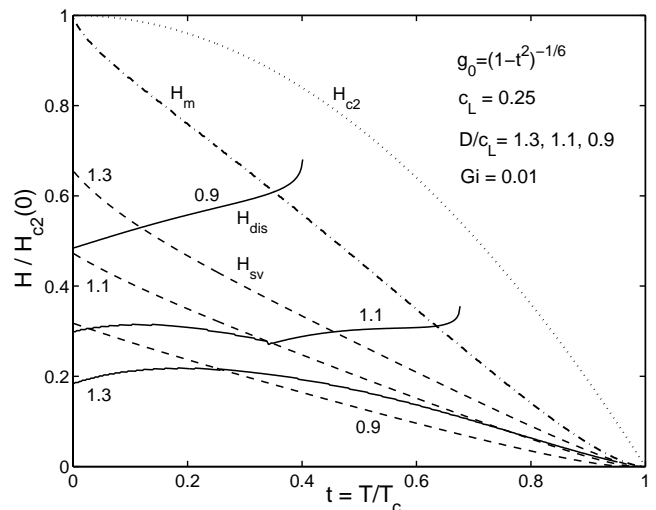
Figure 8. The order–disorder lines $H_{dis}(t)$ (solid lines) and single-vortex pinning boundaries $H_{sv}(t)$ (dashed lines) for three pinning strengths $D/c_L = 1.3$, 1.1, 0.9 and Ginzburg number $Gi = 0.01$. Assumed was δT_c pinning. The dash-dotted line is the melting line $H_m(t)$ and the dotted line shows $H_{c2}(t) = H_{c2}(0)(1 - t^2)$.

VI. Continuum Description of the Vortex State

If one is interested only in length scales larger than the vortex spacing a_0, one may use a continuum description of the vortex state to calculate the distributions of magnetic field and current in superconductors of arbitrary shape. Two different algorithms where presented

[21, 22] which in principle allow to compute the electromagnetic behavior of superconductors of arbitrary shape with and without vortex pinning. The extension to finite London depth λ is given in [5].

Apart from the Maxwell equations, a continuum description requires the constitutive laws of the superconductor. These may be obtained, e.g., from the London theory, Sct. II, by taking the limits $a_0 \to 0$ and $\lambda \to 0$ (or keeping finite λ [5]), and from appropriate models of vortex dynamics. One constitutive law is the reversible magnetization curve of a pin-free superconductor, $M(H)$ or $\bar{B}(H) = \mu_0 H + \mu_0 M(H)$, where H is an effective applied field which would be in equilibrium with the local induction $\bar{B}$. In the simplest case this law may read $M = 0$ or $\bar{B} = \mu_0 H$, valid if everywhere $\bar{B}$ is larger than several times the lower critical field B_{c1}. But in general the reversible $M(H)$ computed from London or GL theories should be used, as discussed in [21, 22, 23, 24].

When the finite lower critical field H_{c1} is accounted for, the magnetization curve $M(H_a)$ in general is irreversible (i.e. a loop) even in complete absence of vortex pinning. This pin-free irreversibility is caused by a geometric barrier for the penetration of magnetic flux, which is absent only if the superconductor has the shape of an ellipsoid or if it has a sharp edge or cusp, at which the applied field H_a is strongly enhanced such that flux lines can penetrate easily. For example, in superconducting cylinders or strips with rectangular cross section $2a \times 2b$ ($2a$ = diameter or width, $2b$ = height) in increasing H_a, the magnetic flux penetrates first reversibly at the four corners in form of nearly straight flux lines, see Figs. 4, 9. When the field of first flux entry B_{en} is reached, these flux lines join at the equator, contract, and jump to the specimen center, from where they gradually fill the entire superconductor. When H_a is decreased again, some flux exits first reversibly, but below a reversibility field $H_{rev} > H_{en}$ the magnetization loop opens, see Fig. 10, since the barrier for flux exit is absent or weaker than the barrier for flux entry. For arbitrary aspect ratio b/a the entry field is [22, 24]

$$H_{en} \approx H_{c1} \tanh \sqrt{cb/a}, \qquad (18)$$

where $c = 0.36$ for strips and $c = 0.67$ for disks or cylinders. This geometric barrier should not be confused with the Bean-Livingstone barrier for the penetration of a straight vortex line into the planar surface of a superconductor, which would lead to a similar asymmetric magnetization loop. The geometric barrier is caused by the line tension of the vortices penetrating at sharp [21, 22, 24] or rounded [25] corners. This line tension P (see Sct. IV) is balanced by the Lorentz force exerted on the vortex ends by the surface screening currents and directed towards the specimen center. The irreversible magnetic behavior of thin strips with an edge barrier (and without or with bulk pinning) in perpendicular H_a was calculated analytically by Zeldov et al. [26].
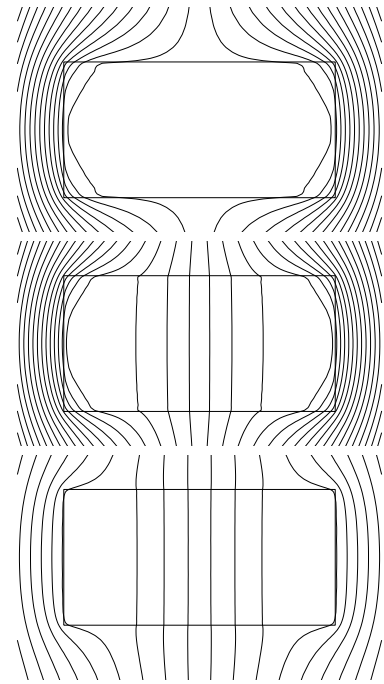
Pin–free strip at H_a/H_{c1} = 0.38, 0.44, 0.20

Figure 9. The magnetic field lines in and near a pin-free strip of aspect ratio $b/a = 0.5$ in an increasing applied perpendicular field H_a at two field values $H_a/H_{c1} = 0.38$ (top) and 0.44 (middle) just below and above the entry field $H_{en} = 0.40 H_{c1}$, and in decreasing field at $H_a/H_{c1} = 0.20$ (bottom).
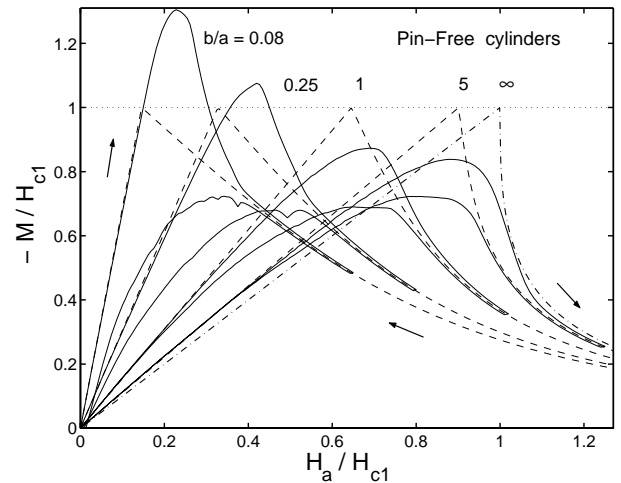

Figure 10. Irreversible magnetization of pin-free cylinders with various aspect ratios $b/a = 0.08$ (thin disk) to ∞ (long cylinder) in a cycled axial magnetic field H_a (solid lines). The dashed lines show the reversible magnetization curves of ellipsoids chosen such that they have the same initial slope $1/(1 - N)$ as the corresponding cylinder.

The computed irreversible magnetization loops of pin-free superconductor cylinders with various aspect ratios $b/a = 0.08$ (thin disk) to $b/a = \infty$ (long cylinder) in an axial field H_a are depicted in Fig. 10, together

with the corresponding reversible magnetization curves of ellipsoids which have the same initial slope (Meissner state) as the cylinders. These magnetization loops of cylinders (like those of other non-ellipsoids) have a maximum at $H_a \approx H_{en}$, and at $H_a > H_{rev}$ they are reversible and coincide with the magnetization of the corresponding ellipsoid. All pin-free magnetization loops are symmetric, $M(-H_a) = -M(H_a)$ with $M(0) = 0$, i.e., no remanent flux can remain at $H_a = 0$ since bulk pinning is absent and there is no barrier for flux exit when $H_a = 0$. Fig. 11 shows magnetization curves of a short cylinder with finite H_{c1} for various strengths of bulk pinning.
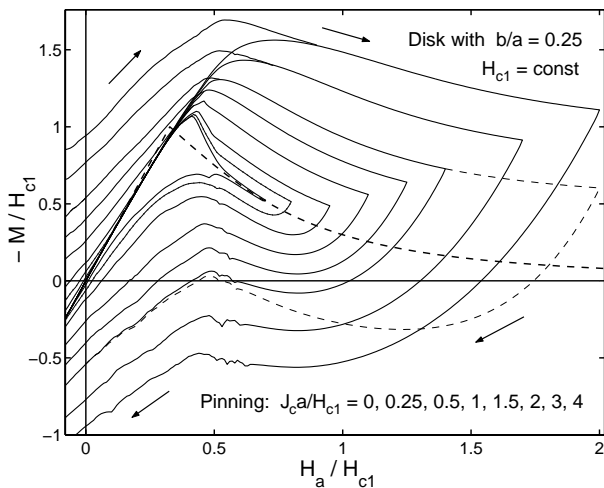

Figure 11. Magnetization loops of a thick disk with aspect ratio $b/a = 0.25$ and constant H_{c1} but various pinning strengths $J_c = 0.25, 0.5, 1, 1.5, 2, 3, 4$ in units H_{c1}/a and for various sweep amplitudes of the applied field H_a. Bean model, i.e., the critical current density J_c is independent of the induction B. The inner loop belongs to the pin-free disk and the outer loop to strongest pinning ($J_c = 4$). The bold dashed line shows the reversible magnetization of the corresponding ellipsoid.

The reversible magnetization curves of pin-free ellipsoids $M(H_a, N)$ follow from the magnetization curve $M(H_a, N = 0) = \bar{B}/\mu_0 - H_a$ of long cylinders in parallel field H_a by the concept of a demagnetization factor N. One has $0 \le N \le 1$, $N = 0$ for parallel geometry, $N = 1/2$ for infinite cylinders in perpendicular field, $N = 1/3$ for spheres, and $N = 1$ for thin films in perpendicular field. For ellipsoids with $N \ne 0$ one has to solve the implicit equation for an effective internal field H_i [24],

$$H_i = H_a - NM(H_i, N = 0),\qquad(19)$$

to obtain the reversible magnetization $M(H_a, N) = M(H_i, N = 0)$ (dashed lines in Fig. 10) from the $M(H_a, N = 0)$ of longitudinal geometry. In particular, in the Meissner state ($\bar{B} \equiv 0$) one has $M(H_a, 0) = -H_a$ and $M(H_a, N) = -H_i = -H_a/(1 - N)$ for $|H_a| \le (1 - N)H_{c1}$.

As a second constitutive law one may use the local electric field $\mathbf{E} = \mathbf{E}_v(\mathbf{J}, \mathbf{B})$ which is generated by

moving vortices and which in a compact way can describe free flux flow and Hall effect, but also vortex pinning and thermally activated depinning or creep. A simple but still quite general isotropic model is $\mathbf{E}_v = \rho(J, B)\mathbf{J}$ with $\rho = \text{const} \cdot B \cdot (J/J_c)^{n-1}$, where J_c is the critical current density and n the creep exponent [5, 27]. This realistic model means an activation energy $U(J) = U_0 \ln(J_c/J)$ for depinning that enters in $E = E_c \exp[-U(J)/kT] = E_c(J/J_c)^n$ with $n = U_0/kT$. Within this model, flux flow is described by $n = 1$, flux creep (relaxation with approximately logarithmic time law) by $n \gg 1$, and Bean's critical state model of vortex pinning by the limit $n \to \infty$. In general, both J_c and n may depend on the local induction $\bar{B}$ and on the temperature T. Fig. 12 shows some magnetization loops of a short cylinder calculated in [27] for two different $J_c(B)$ models and two creep exponents. For the electrodynamics of thin strips, disks, and rings in a perpendicular field see [28, 29, 30], and for thin rectangles and films of other shapes see [31, 32]. Thin strips in perpendicular dc and ac magnetic fields and with transport current are considered in [33]. Analytic and numerical solutions were also obtained for flux expulsion and penetration into thin strips with a bend along the middle line [34] and for thin shells (or hats) of conical shape [35].
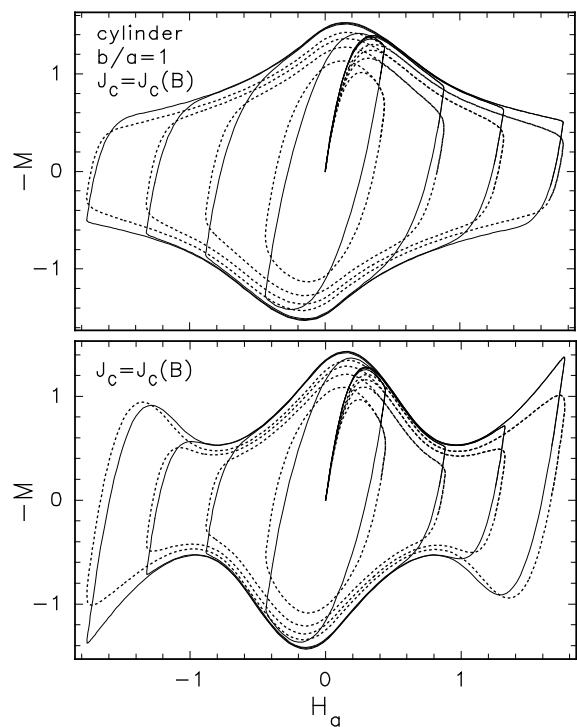

Figure 12. Magnetization loops of cylinders with aspect ratio $b/a = 1$, creep exponents $n = 51$ (bold lines) and $n = 5$ (dashed lines), with $B_{c1} = 0$, in sinusoidally cycled applied field H_a for two induction dependent critical current densities $J_c(B) = J_{c0}/(1 + 3\beta)$ (top, Kim model) and $J_c(B) = J_{c0}(1 - 3\beta + 3\beta^2)$ (bottom, a "fish-tail" model), where $\beta = |B|/B_p$, $B_p = 0.88\mu_0 J_{c0}a$. The magnetization M is in units $J_{c0}a/(2\pi)$ and H_a in units $J_{c0}a$, where a, b are the radius and half height of the cylinder.

In all these calculations the London depth λ was assumed to be negligibly small. Finite λ may be accounted for by modifying the current–voltage law, using $\mathbf{E} = \mathbf{E}_v(\mathbf{J}, \mathbf{B}) + \mu_0 \lambda^2 \partial \mathbf{j}/\partial t$ [5]. Here the first term is generated by moving vortices and the second term describes the Meissner surface currents [4, 5].

References

1. P.G. DeGennes, *Superconductivity of Metals and Alloys*, New York, Benjamin, 1966.

2. M. Tinkham, *Introduction to Superconductivity,* New York, McGraw-Hill, 1975.

3. E.H. Brandt, Rep. Progr. Phys. **58** (1995) 1465-1594.

4. E.H. Brandt and G.P. Mikitik, Phys. Rev. Lett. **85** (2000) 4164.

5. E.H. Brandt, Phys. Rev. B **64** (2001) 024505, 1-15.

6. J.R. Clem, J. Low Temp. Phys. **18** (1975) 427.

7. Z. Hao, J.R. Clem, M.W. Mc Elfresh, L. Civale, A.P. Malozemov, F. Holtzberg, Phys. Rev. B **43** (1991) 2844.

8. E.H. Brandt, Phys. Rev. Lett. **78** (1997) 2208.

9. E.H. Brandt, J. Low Temp. Phys. **42** (1981) 557.

10. Jung-Chun Wei, Tzong-Yer Yang, Jpn. J. Appl. Phys. **35** (1996) 5696.

11. G. Carneiro, E.H. Brandt, Phys. Rev. B **61** (2000) 6370.

12. J.R. Clem, Phys. Rev. B **43** (1991) 7837.

13. E.H. Brandt, Phys. Rev. B **34** (1986) 6514.

14. A.A. Abrikosov, L.P. Gorkov, I.E. Dzyaloshinski, *Methods of Quantum Field Theory in Statistical Physics*, Englewood Cliffs, Prentice Hall, 1963.

15. V.G. Kogan et al., Phys. Rev. B **54** (1996) 12386.

16. E.H. Brandt, U. Essmann, phys. stat. sol. (b) **144** (1987) 13.

17. E.H. Brandt, Phys. Stat. Sol. b, **77** (1976) 709.

18. I.M. Babich, Yu.V. Sharlai, G.P. Mikitik, Fiz. Nizk. Temp. **20** (1994) 227 [Low Temp. Phys. **20** (1994) 220].

19. G. Blatter, M.V. Feigel'man, V.B. Geshkenbein, A.I. Larkin, V.M. Vinokur, Rev. Mod. Phys. **66** (1994) 1125.

20. G.P. Mikitik, E.H. Brandt, Phys. Rev. B **64** 184514 (2001), 1-14.

21. R. Labusch, T.B. Doyle, Physica C **290** (1997) 143.

22. E.H. Brandt, Phys. Rev. B **59** (1999) 3369.

23. T. Hocquet, P. Mathieu and Y. Simon, Phys. Rev. B **46** (1992) 1061.

24. E.H. Brandt, Phys. Rev. B **60** (1999) 11939.

25. M. Benkraouda, J.R. Clem, Phys. Rev. B **58** (1998) 15103.

26. E. Zeldov, A.I. Larkin, V.B. Geshkenbein, M. Konczykowski, D. Majer, B. Khaykovich, V.M. Vinokur, H. Strikhman, Phys. Rev. Lett. **73** (1994) 1428.

27. E.H. Brandt, Phys. Rev. B **58** (1998) 6506.

28. E.H. Brandt, Phys. Rev. B **50** (1994) 4034.

29. D.V. Shantsev, Y.M. Galperin, T.H. Johansen, Phys. Rev. B **60** (1999) 13112.

30. E.H. Brandt, Phys. Rev. B **55** (1997) 14513.

31. L. Prigozhin, J. Comput. Phys. **144** (1998) 180.

32. E.H. Brandt, Phys. Rev. B **52** (1995) 15442.

33. G.M. Mikitik and E.H. Brandt, Phys. Rev. B **64** (2001) 092502, 1-4.

34. Leonardo R.E. Cabral and J. Albino Aguilar, Physica C **341-348**, 1049 (2000).

35. Leonardo R.E. Cabral, Thesis, Universidade Federal de Pernambuco, Recife (2001).